

Uniaxial incommensurate rare-gas-monolayer solids. I. Structure and statistical mechanics

J. M. Gottlieb and L. W. Bruch

Department of Physics, University of Wisconsin—Madison, Madison, Wisconsin 53706

(Received 28 February 1991)

Calculations are reported for uniaxial incommensurate solid phases of rare-gas monolayers adsorbed on triangular substrate surfaces. The monolayer is treated in a two-dimensional approximation with adatom-adatom pair potentials and a periodic adatom-substrate corrugation potential. The two signs of the substrate corrugation amplitude lead to solutions with different diffraction signatures. Structures are determined in the zero-temperature classical approximation and energies are calculated in the classical and quasiharmonic approximations. The energy of a domain wall is calculated as a function of temperature and the phase transition between commensurate and incommensurate lattices is treated. The in-plane motion of the domain walls is analyzed in terms of the Peierls barrier energy and the frequency spectrum of the monolayer for wave vectors in the direction of the misfit.

I. INTRODUCTION

In a physisorbed rare-gas solid, the behavior of the adlayer is strongly influenced by the competition between the adatom-adatom and the adatom-substrate interactions.¹⁻³ The interplay leads to a fascinating hierarchy of different solid phases and phase transitions between them. One very significant solid phase is the uniaxial incommensurate (UIC) lattice,¹ with an average compression in only one spatial direction. At small misfits it consists of a lattice of well-defined domain walls which are parallel on the average. It has been proposed¹ as a major step in the evolution of the monolayer from commensurate to incommensurate lattices. It is tractable enough to permit a detailed theoretical treatment,⁴⁻⁶ including thermal effects, and is an excellent testing ground for the comparison between theory and experiment of nonuniform adsorbed layers.

Here the Helmholtz free energy and the grand potential are computed for a model of the UIC monolayer which is designed to (i) allow study of both UIC lattices and commensurate ($\sqrt{3} \times \sqrt{3}$)R30° (C) lattices on the triangular surface lattice, (ii) allow investigation of the UIC-C phase transition by changes of the thermodynamic variables and of the model parameters, (iii) allow study of both strongly and weakly modulated UIC lattices, (iv) use simple, yet reasonably accurate, interaction models, and (v) provide for a domain structure of adjustable repeat length. The total potential energy is minimized as a function of the internal structural parameters. Then the normal mode frequencies are evaluated and the free energy is computed in the quasiharmonic approximation. The derived information includes data for the structure, energy, and dynamics of the UIC lattice.

There are two broad classes of low-energy UIC structures⁷ in this work. In one structure, the compressed domain walls are characterized by one-component displacement vectors. Kardar and Berker⁷ named them superheavy walls, and Gooding, Joos, and Bergersen⁴ and Gordon and Lancon⁵ studied examples in models of krypton adsorbed on graphite. In the other structure,⁶ the

compressed walls have two-component displacement vectors and are a generalization of the Kardar and Berker⁷ heavy walls. They arise for models in which the minimum-energy adsorption sites are at threefold-coordination sites of the surface triangular lattice cell and were first identified by Gottlieb.⁶

There are two situations for the occurrence of the UIC-C phase transition. First, the ordering of the minimum free energies changes as the temperature is varied. For instance, in cases where the commensurate lattice has lower density than the minimum-energy lattice for the adatom-adatom interactions, the monolayer may thermally expand to the commensurate lattice.⁸ Black and Janzen⁹ explored this possibility in molecular-dynamics simulations of xenon adsorbed on the (111) face of platinum, Xe/Pt(111). Second, at a given temperature, as the chemical potential is increased the C-UIC transition may be driven by mechanical compression.¹⁰ The relation of the chemical potential increase to the energy of isolated domain walls is developed here. The analysis corresponds to a mean-field theory and the UIC-C phase transition is continuous, consistent with the general discussion of Bak *et al.*¹

The Peierls barrier energy^{11,12} for translation of the UIC domains is calculated as a function of model parameters and is found to be closely correlated to the smallest normal-mode frequency at the Brillouin-zone center, as suggested by Black and Mills.¹³ This is an extensive study of these properties for a model of a physisorbed monolayer.

In the following paper,¹⁴ the methods developed here are applied to an analysis of the UIC lattice of monolayer Xe/Pt(111). Diffraction data¹⁵ indicate⁶ that Xe/Pt(111) has superheavy walls and not the modified heavy walls expected for a lattice obtained by compression of a commensurate lattice with adatoms located in the threefold positions of an fcc (111) surface.

The organization of this paper is as follows: Section II contains the formulation of the calculations and Sec. III contains results for the properties of the UIC lattices. Section IV contains concluding remarks.

II. FORMULATION

A. Equilibrium

The condition for equilibrium of an adsorbed layer, on area A and at temperature T , which coexists with a three-dimensional gas at chemical potential μ and the same temperature is that the grand potential

$$\Omega = F_a(\bar{N}_a) - \mu \bar{N}_a, \quad (2.1)$$

be a minimum.³ In Eq. (2.1), F_a is the Helmholtz free energy of the N_a adatoms; the density N_a/A and internal structural parameters of the monolayer are to be adjusted to minimize Ω . The substrate is assumed to be rigid and inert and the (dilute) three-dimensional gas and the monolayer are assumed to be distinct separated phases.

B. Statistical mechanics

The Helmholtz free energy is constructed for the UIC and C monolayer solids in the presence of a rigid substrate surface which has a triangular Bravais lattice.⁸ The monolayer is idealized by limiting the complexity of the structures and interactions; then approximations are made in evaluating the free energy.

The lowest-order approximation to the free energy is the static potential energy. This is minimized with respect to variations of the internal structural parameters, using a classical force relaxation technique. Then the normal-mode frequencies are found for small-amplitude oscillations about the minimum potential energy configuration. The zero-temperature (0 K) approximation consists of adding the zero-point oscillator energy to the potential energy. The quasiharmonic free energy consists of the sum of the static potential energy and the dynamical free energy of the normal modes. The free energy is incompletely minimized because the structural optimization is performed only on the static potential energy.

For the dynamical free energy, the sum over wave vectors in the first Brillouin zone of the domain superlattice is performed with the method of special points. Cunningham's 16-point set¹⁶ for the rectangular lattice is used, including a reduction which arises because of the symmetries of the domain basis.¹⁷ For the triangular (C) lattice,¹⁶ a 45-point set is used. The largest eigenvalue problem in this work is that of a 96×96 Hermitian dynamical matrix for a UIC domain of 48 rows.

C. Atomic model

The geometry of the substrate surface is shown in Figs. 1 and 2. The surface has a triangular Bravais lattice with unit cell of side L ; the vertices of the hexagons are threefold-coordination positions of the Bravais cells. In Fig. 1, the hexagon centers are minimum-energy adsorption sites. This arises in models used for spherical adsorbates on graphite;³⁻⁵ the vertices then correspond to surface carbon atoms. In Fig. 2, the two sets of threefold positions are degenerate minimum-energy adsorption sites. This arises in simple models^{6,18} for spherical adsorbates on the (111) face of an fcc solid, but the situation for Xe/Pt(111) appears to be more complex.^{6,19} In both

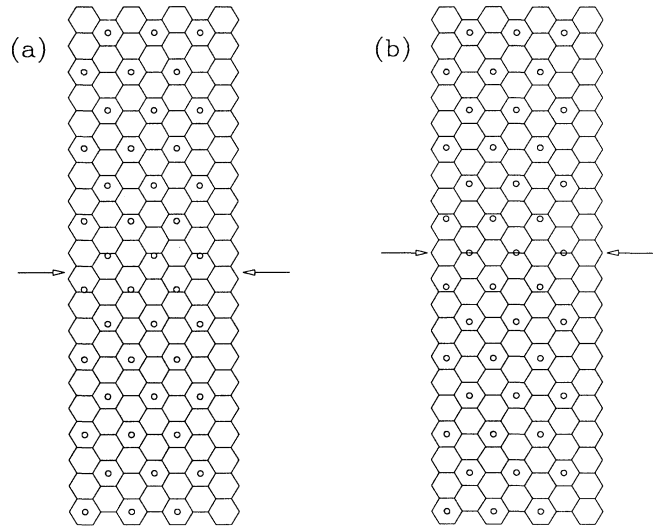


FIG. 1. Examples of even- l UIC $V_g < 0$ lattices. The arrows indicate the symmetry lines of the domains. $l=14$, $\sigma=4.0$ Å, and $V_g=-20$ K. Vertices of the background hexagons represent either carbon sites of the basal plane surface of graphite or the threefold-coordination positions of the Bravais unit cell of an fcc (111) surface. (a) Stable configuration; (b) unstable configuration.

cases, bridge sites of the adsorption energy surface are located at midpoints of the hexagon sides.

The potential energy of the adlayer is written as a sum of the adatom-adatom and the adatom-substrate interactions. Phenomenological forms are used, and the parameters include such processes as substrate-mediated interactions to some extent.

The adatom-adatom interaction is taken to be the sum of Lennard-Jones (12,6) pair potentials

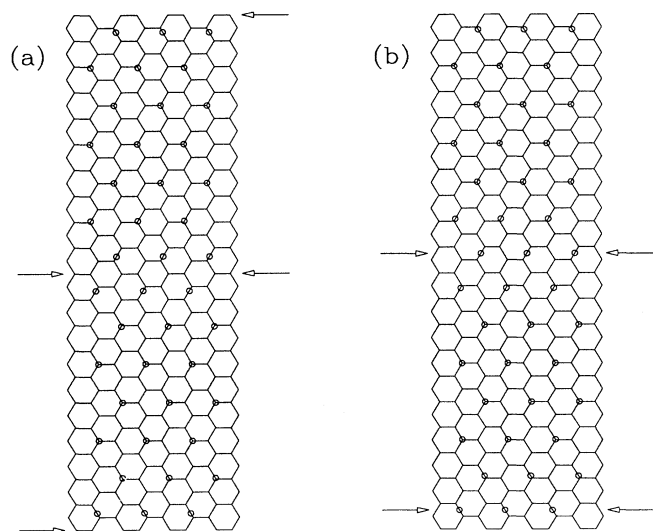


FIG. 2. Examples of even- l UIC $V_g > 0$ lattices. $l=14$, $\sigma=4.0$ Å, and $V_g=180$ K. Identifications as in Fig. 1. (a) Stable configuration; (b) unstable configuration.

$$\phi(r) = 4\epsilon \left[\left(\frac{\sigma}{r} \right)^{12} - \left(\frac{\sigma}{r} \right)^6 \right]. \quad (2.2)$$

Equation (2.2) is a convenient and reasonably accurate representation of the force between rare-gas atoms; estimates for ϵ and σ may be obtained from three-dimensional data,²⁰ but they are adjustable parameters here.

The adatom-substrate interaction can be reduced by plausible approximations to a function with a small number of parameters. Steele's Fourier decomposition¹⁸ for the translational symmetry leads to an expression with a single energy parameter V_g if the monolayer remains close to the overlayer distance set by the average holding potential, and effects of underlying substrate layers are ignored¹⁸ in the lateral energy variations. Then the adatom-substrate potential energy for atoms in the two-dimensional monolayer solid is

$$V(r) = V_g \sum_g \exp(i\mathbf{g} \cdot \mathbf{r}), \quad (2.3)$$

where the sum is over the six shortest reciprocal-lattice vectors of the substrate Bravais lattice of length $g_0 = 4\pi/L\sqrt{3}$. The two sets of threefold sites have equal energies with the approximations used for Eq. (2.3). Truncation of the Fourier series at the first shell of reciprocal-lattice vectors is rationalized by Steele's result¹⁸ that for many models the magnitude of the amplitudes V_g at the equilibrium height decreases rapidly for larger g .

The sign of V_g determines the locations of the minima of $V(r)$. For $V_g < 0$, there is one minimum per Bravais cell, located at the hexagon centers in Fig. 1. For $V_g > 0$ there are two degenerate minima per Bravais cell, located at the hexagon vertices in Fig. 2.

The model calculations are designed to explore possible structures of Xe/Pt(111) and some parameters are held fixed or varied over a small range. The length L is held at 2.77 Å, the nearest-neighbor spacing in platinum. The energy scale of the Lennard-Jones (12,6) potential is held at $\epsilon = 230$ K, a value used for xenon;²⁰ this is discussed further in the following paper.¹⁴ The length scale σ is varied in the range 4.0–4.10 Å, near values used for xenon. The amplitude V_g is varied over large ranges. For the dynamical properties the atomic mass is 217.9×10^{-24} g, for xenon. Adatom-adatom interactions are retained for a total of 36 neighbors of each atom.

D. Adlayer structures

The commensurate ($\sqrt{3} \times \sqrt{3}$) $R30^\circ$ (C) monolayer lattice has a lattice constant $L_c = \sqrt{3}L$ ($= 4.80$ Å for Pt) and is illustrated by that portion of Fig. 1 for which the adatoms (circles) are in hexagon centers. Another example is the upper portion of the domains in Fig. 2.

The uniaxial incommensurate (UIC) lattice, examples of which are shown in Figs. 1–3, is the principal subject of this paper. The adlayer atoms form periodically repeating domains of l rows oriented parallel to the horizontal (x) axis in the figures. The separation of atoms in each row is equal to the commensurate lattice constant

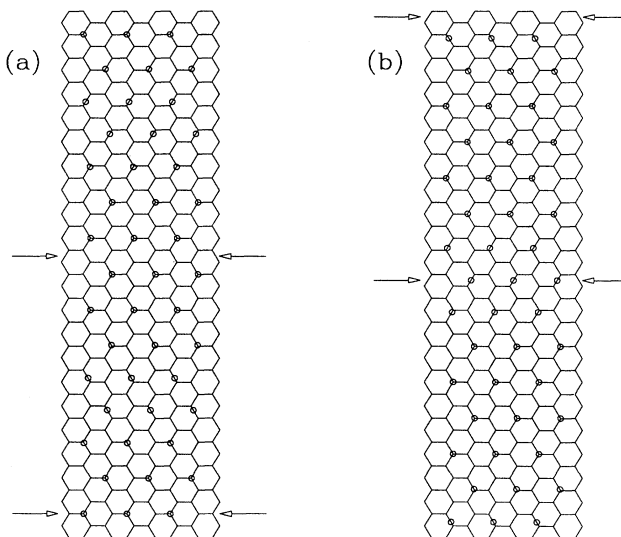


FIG. 3. Examples of odd- l UIC $V_g > 0$ lattices. $l = 13$, $\sigma = 4.0$ Å, and $V_g = 180$ K. Identifications as in Fig. 1. (a) Stable configuration; (b) unstable configuration.

L_c . Along the vertical (y) axis, a compression of one substrate spacing L relative to the commensurate lattice is applied to each domain as a whole. The average row spacing in the UIC lattice is

$$d = (3L/2)(1 - \bar{m}), \quad (2.4)$$

where \bar{m} is the mean misfit and is given in terms of the domain size by $\bar{m} = (2/3l)$. A weakly modulated UIC lattice has only small distortions from the uniform UIC lattice with equally spaced rows. For the well-developed domains at small misfit, positions are expressed in terms of displacements from the commensurate lattice positions \mathbf{R}_{mn} by

$$\mathbf{r}_j = \mathbf{R}_{mn}(C) + \boldsymbol{\eta}_j, \quad (2.5)$$

where the vector displacement $\boldsymbol{\eta}$ depends only on the row index j of the commensurate lattice. An example of the displacements is shown in Fig. 4. The adlayer is placed relative to the substrate by specifying the origin of the lattice \mathbf{R}_{mn} relative to the substrate.

Two different UIC lattice configurations are defined,¹¹ termed stable and unstable. The stable configuration is required to have at least one symmetry line which lies between two rows; it is expected to have the minimum potential energy.²¹ The unstable configuration is distinguished from the stable one in that all adatoms in at least one selected row are required to be above bridge sites of the substrate potential energy; that row is a symmetry line of the structure. Examples of stable-unstable pairs are shown in Figs. 1–3. The difference in the displacements for one pair is shown in Fig. 5. The potential energy difference between members of a pair^{11,13} is defined to be the Peierls barrier energy; it is found here to be rather small for a physisorbed monolayer.

The UIC configurations for the $V_g < 0$ case are constructed in close analogy to Joos's treatment¹¹ of the

one-dimensional Frenkel-Kontorova chain with even and odd numbers of atoms in the domain. The stable-unstable pair for even l is shown in Fig. 1. The construction for the $V_g > 0$ case is more complicated: pairs for even and odd l are shown in Figs. 2 and 3, respectively. Eight UIC lattice cases (two signs of V_g , stable-unstable, even-odd l) are optimized: an iterative set of small atomic displacements starting from an appropriately placed uniform UIC lattice leads to rapid convergence in all except the $V_g > 0$, stable, odd l case.

III. PROPERTIES

The constructions lead to two main categories of properties of the UIC lattices, characterizing the structure and the energy. As noted, the structural properties are all based on a minimization of the static potential energy.

A. Structural properties

The displacements for a UIC lattice with small misfit are distributed quite nonuniformly over the domain, as shown in Figs. 4 and 5. The region in which most of the

displacement occurs is termed the domain wall. The domain wall width is defined with the construction shown in Fig. 4, a linear extrapolation from the midpoint to the asymptotes of each riser. This is the definition of Gordon and Lancon⁵ and results for the $V_g < 0$ cases agree with theirs. Results for the $V_g > 0$ case are shown in Fig. 6. The $V_g < 0$ cases have the displacements confined to the y direction, but in the $V_g > 0$ cases the net uniaxial compression is subdivided into two domain wall regions which are displaced from each other along the x direction. These qualitative differences arise from the different surface topographies: the UIC lattice samples both sets of threefold positions of the surface cells for $V_g > 0$.

The width of the domain wall is a measure of how nonuniform the lattice is. As the domain size l is increased, the width approaches a limit for each set of interaction parameters, indicating that the domain walls become isolated. The results in Fig. 6 are shown as ratios to widths derived from a variational treatment²² of the continuum theory of such walls. If the continuum theory were accurate, the ratios would be 1. The trends and the sizes of the ratios are similar to those found by Gordon

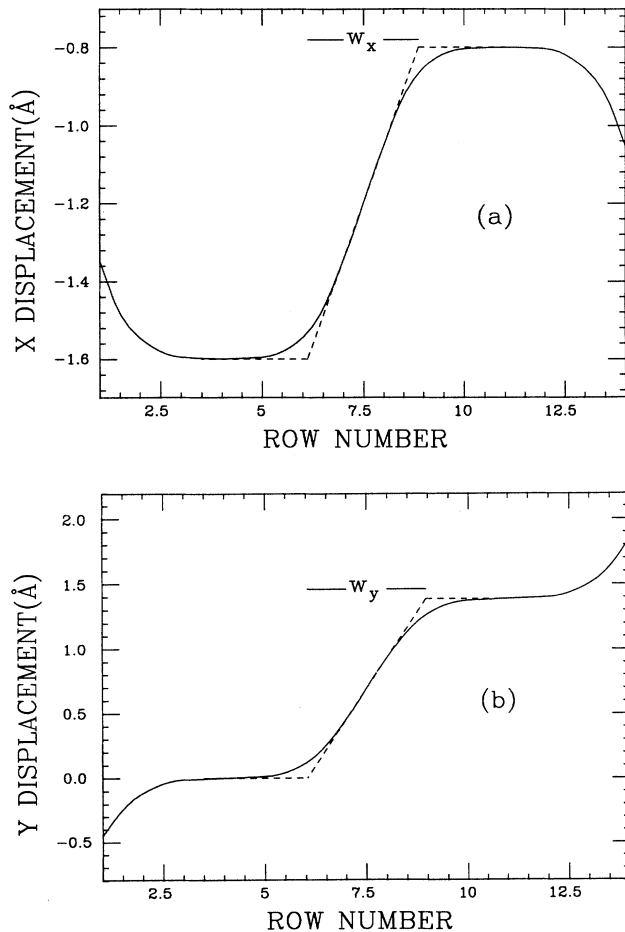


FIG. 4. Adatom displacements and domain-wall definition for $V_g > 0$ UIC lattice. $l = 14$, $\sigma = 4.0$ Å, and $V_g = 180$ K. Components of displacement, Eq. (2.5); actual atomic positions correspond to integer values of the row number.

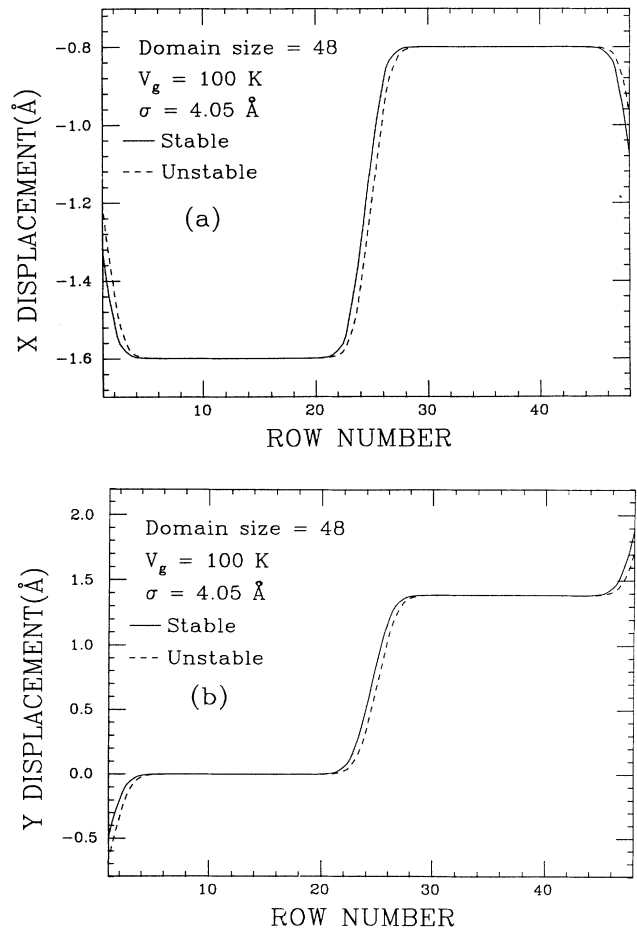


FIG. 5. Adatom displacements for optimized stable and unstable UIC lattice. $l = 48$, $\sigma = 4.05$ Å, and $V_g = 100$ K. The x and y components of the displacement, Eq. (2.5), are shown as a function of the (integer) row number.

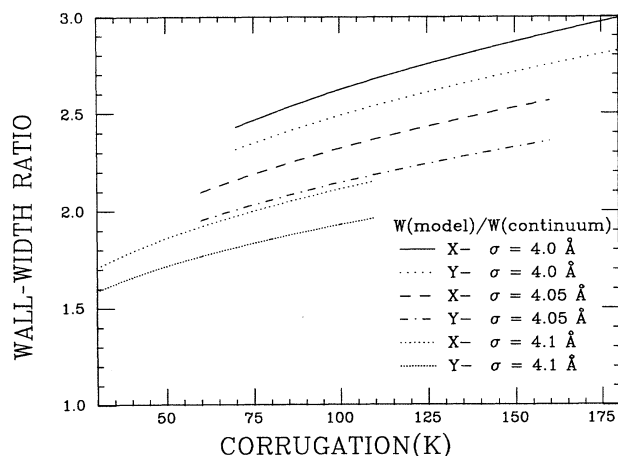


FIG. 6. Variation of the domain wall widths for $V_g > 0$. The ratio of the wall widths derived from the construction shown in Fig. 4 to the widths calculated in a continuum approximation is plotted as a function of corrugation amplitude V_g for three values of σ . The domains have $l=48$. Departures of the ratios from 1 and the trend with V_g reflect the errors which arise in the continuum approximation (Ref. 22) by using the elastic constants at the commensurate density as the average elastic constants of the adlayer.

and Lancon⁵ for a model of krypton on graphite. In both instances, the commensurate lattice is quite dilated relative to the intrinsic triangular lattice set by the adatom-adatom potentials and there is ambiguity as to the choice of average elastic constants for the adlayer.

The smallest atomic spacing in the UIC lattice gives information on the internal structure of domain walls. The difference between it and the commensurate spacing L_c ($=4.80 \text{ \AA}$) is a measure of the range of conditions within a single domain. In this work the difference is 5–10 % of L_c . Also, if the spacing is smaller than the nearest-neighbor spacing in the low-pressure three-dimensional (3D) adatom lattice, there is a highly stressed region of the domain which might relax by motions perpendicular to the monolayer plane. Here the most strongly modulated (largest V_g and smallest σ) lattices have smallest spacings which are a few percent less than the nearest-neighbor spacings of the corresponding 3D Lennard-Jones lattices.

The structure factor gives the signature of the lattice in a diffraction experiment. For wave vectors \mathbf{q} in the plane of the monolayer, it is defined by

$$S(\mathbf{q}) = \left| \frac{1}{l} \sum_j e^{i\mathbf{q} \cdot \mathbf{r}_j} \right|^2, \quad (3.1)$$

where \mathbf{r}_j is the position of the j th row in the UIC lattice and the sum is over the l rows in the domain. The wave vectors \mathbf{q} are reciprocal-lattice vectors of the domain supercell. For weakly modulated lattices only those \mathbf{q} which are in the reciprocal lattice of the uniform UIC lattice have sizable structure factors. The modulation of the adlayer by the holding potential increases as the magnitude of the misfit decreases and an example is shown in the following paper.¹⁴ The subdivided domain walls illus-

trated in Figs. 4 and 5 have characteristic structure factor extinctions⁶ which are not observed in data for Xe/Pt(111).¹⁵

B. Energies

The energy (potential energy or free energy) is calculated as a function of the misfit and is used to evaluate such properties as the energy per unit length of a domain wall and the compressibility. Figure 7 shows the results for one choice of adatom-adatom potential parameters and three choices of the corrugation amplitude. The values of the misfit correspond to integer values of domain size l . All the cases treated in this work have the pattern shown in Fig. 7: the minimum is at zero misfit for small magnitude of V_g and increases continuously from zero as V_g increases beyond a threshold value.

For many of the following calculations, the energy is treated as a smooth function of misfit, assuming that values of the misfit which are not of the form $2/3l$ do not introduce jagged behavior.²³ Support for this assumption comes from the evaluation of the Peierls barrier energy at integer values of l : it is much smaller than the wall energy and indicates pinning energies are small in these cases.

The energy per unit length of a domain wall is defined by

$$E_{\text{wall}} = \frac{l}{L_c} [f(\bar{m}) - f(\sqrt{3})], \quad (3.2)$$

where $f(\bar{m})$ and $f(\sqrt{3})$ are (free) energies per adatom of the UIC and C lattices, respectively. It is extracted from the initial slope of plots such as Fig. 7, i.e., conditions where the domain walls are isolated from each other. Gordon and Lancon⁵ studied a similar quantity. A wall-wall interaction energy can be defined in terms of the departure of such plots from linearity.

The grand potential Eq. (2.1) is rewritten as

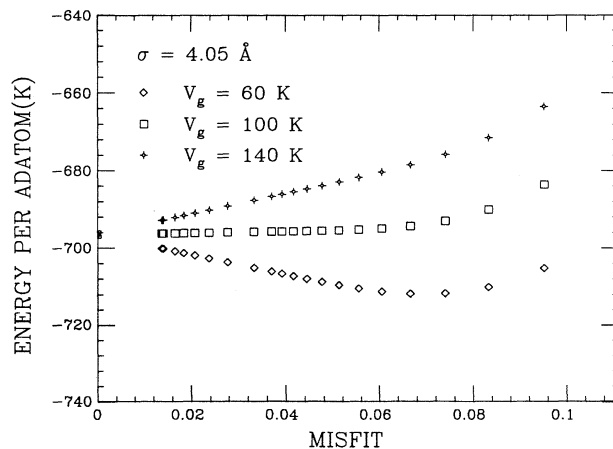


FIG. 7. Potential energy per adatom, measured in K, as a function of misfit for $\sigma=4.05 \text{ \AA}$ and three values of V_g . The zero of energy is the minimum energy of a single adatom on the substrate surface. The points correspond to UIC domains with one unit of misfit over an integer number of rows.

$$\Omega = \bar{N}_a [f(\bar{m}) - \mu], \quad (3.3)$$

and the number of adatoms is expressed in terms of the commensurate lattice number and the misfit by

$$\bar{N}_a = \frac{N_c}{1 - \bar{m}}. \quad (3.4)$$

Then, if the energy $f(\bar{m})$ is a continuous function of the misfit, the condition of minimum grand potential leads to an implicit equation for the equilibrium misfit as a function of the chemical potential

$$\mu = f(\bar{m}) + (1 - \bar{m}) \left[\frac{\partial f(\bar{m})}{\partial \bar{m}} \right]_T. \quad (3.5)$$

The compressibility of the UIC lattice is given by

$$\kappa_T^{-1} = \frac{1 - \bar{m}}{a_c} \left[\frac{\partial^2 f(\bar{m})}{\partial \bar{m}^2} \right]_T, \quad (3.6)$$

where the area of the commensurate cell is $a_c = \sqrt{3}L^2/2$. Clearly, the compressibility is very large in the range of small misfit where the function f is nearly linear.

C. Phase stability

The sign and magnitude of the wall energy E_{wall} are both used to analyze the stability of the C lattice with respect to the UIC lattice. Because the energy as a function of misfit in all cases treated here has the pattern shown in Fig. 7, the C lattice has lower (free) energy than the UIC lattice when the wall energy is positive. Some results for the wall energy as a function of temperature are shown in Fig. 8.

The two situations for the UIC- C phase transition described in Sec. I correspond to distinct paths in the calculated chemical-potential-temperature phase diagram shown in Fig. 9. At sufficiently low temperature the monolayer condenses as a UIC lattice, while at higher temperatures it condenses as a C lattice; the crossover temperature is that for which the wall energy vanishes. Thermal expansion to the UIC- C transition is also discussed by Gordon and Villain.⁸ The second situation occurs for temperatures at which the monolayer condenses as a C lattice: by further increasing the chemical potential beyond the value at condensation, the monolayer may be driven into a UIC lattice. This was observed for Xe/Pt(111) by Kern *et al.*¹⁰

The steps in the second situation are described as follows. If effects of the spreading pressure of the dilute two-dimensional gas are neglected, the chemical potential at monolayer condensation is equal to the free energy per adatom of the C lattice:

$$\mu_c = f(\sqrt{3}). \quad (3.7)$$

The wall energy, Eq. (3.2), gives a linear approximation for $f(\bar{m})$ which suffices to show that a UIC lattice of finite misfit is the phase of minimum grand potential for an increment of chemical potential larger than the threshold

$$\Delta\mu = \frac{3}{2}L_c E_{\text{wall}}. \quad (3.8)$$

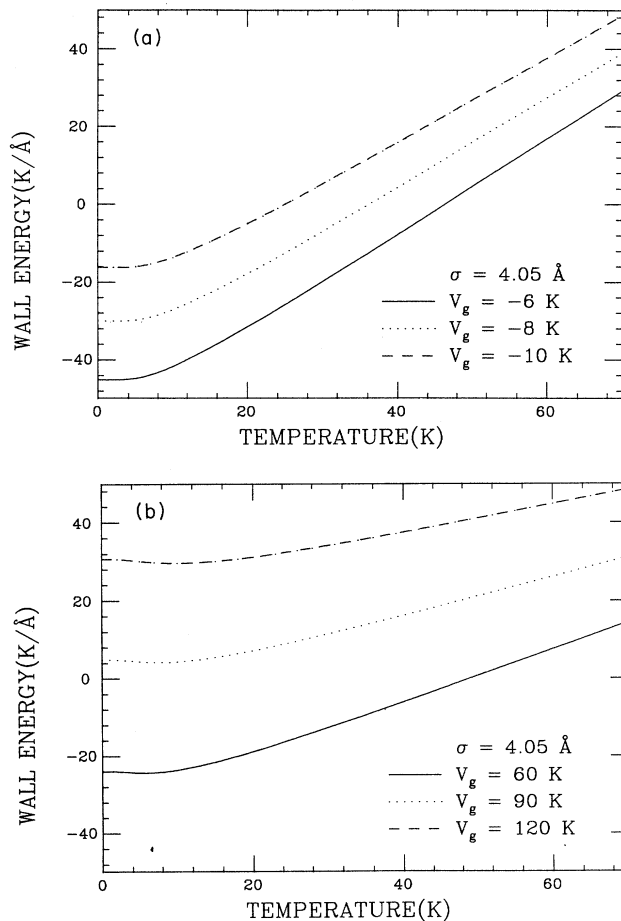


FIG. 8. Domain wall energy, in $\text{K}/\text{\AA}$, as a function of temperature. The wall energy is defined in Eq. (3.2) in terms of the initial slope of the free energy as a function of misfit. The Helmholtz free energy is evaluated in the quasiharmonic approximation. $\sigma = 4.05 \text{ \AA}$, (a) $V_g < 0$; (b) $V_g > 0$.

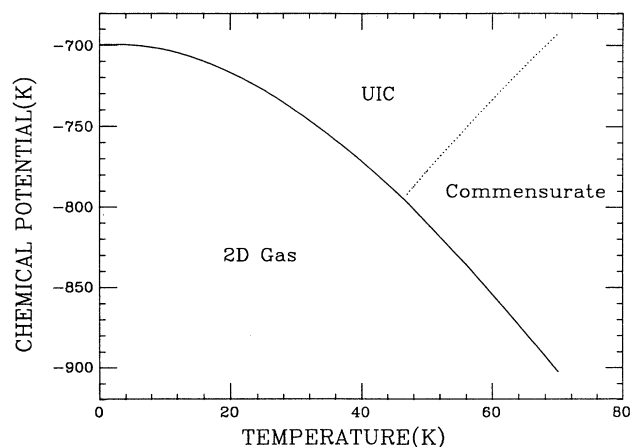


FIG. 9. Calculated chemical potential-temperature phase diagram. $\sigma = 4.05 \text{ \AA}$; $V_g = -6 \text{ K}$. The Helmholtz free energy is calculated in the quasiharmonic approximation and the phase boundaries are determined with the criteria presented in Sec. III C.

For all the interaction parameters used in this work, the C-UIC transition is continuous; when the UIC phase is stable, the grand potential as a function of misfit initially decreases to a minimum before increasing.

The corrugation amplitudes V_g for which the monolayer solid first condenses as a C lattice at 50 K are shown in Table I. Also the values for which the increment $\Delta\mu$ takes on prescribed values at 70 K are shown there. The corresponding values from static potential-energy calculations were presented previously.⁶ Thermal expansion effects reduce the magnitudes of the amplitudes in Table I from those of the previous work.⁶

D. In-plane motion of UIC lattices

The Peierls barrier potential energy V_{Peierls} is defined to be the difference between the potential energies (per column in a domain) of the stable and unstable configurations. It depends on the domain size l and for large l gives an estimate of the energy barrier to translation of a domain wall. The energy V_{Peierls} is shown as a function of V_g in Fig. 10. The semilogarithmic plot of V_{Peierls} as a function of $1/\sqrt{V_g}$ is suggested by results for the Frenkel-Kontorova chain.^{11,12} The definition of V_{Peierls} leads to an irregular dependence on even-odd l for $V_g > 0$: the value for $l=47$ is precisely half that for $l=48$.

For all of the calculations in the quasiharmonic approximation, a full set of normal-mode frequencies is obtained for each parameter set. Two aspects of the spectra are shown in Figs. 11 and 12. The zone-center frequency, defined to be the lowest frequency at zero wave vector, reflects the pinning of the adlayer to the substrate. It is related to the Peierls potential V_{Peierls} and Black and Mills¹³ suggested that V_{Peierls} is roughly proportional to the square of the zone-center frequency. This is confirmed by the dynamic ratio

$$\xi = \frac{M\omega_0^2}{V_{\text{Peierls}}} \quad (3.9)$$

plotted in Fig. 11 for a large domain; M is the adatom mass and ω_0 is the zone-center angular frequency. The

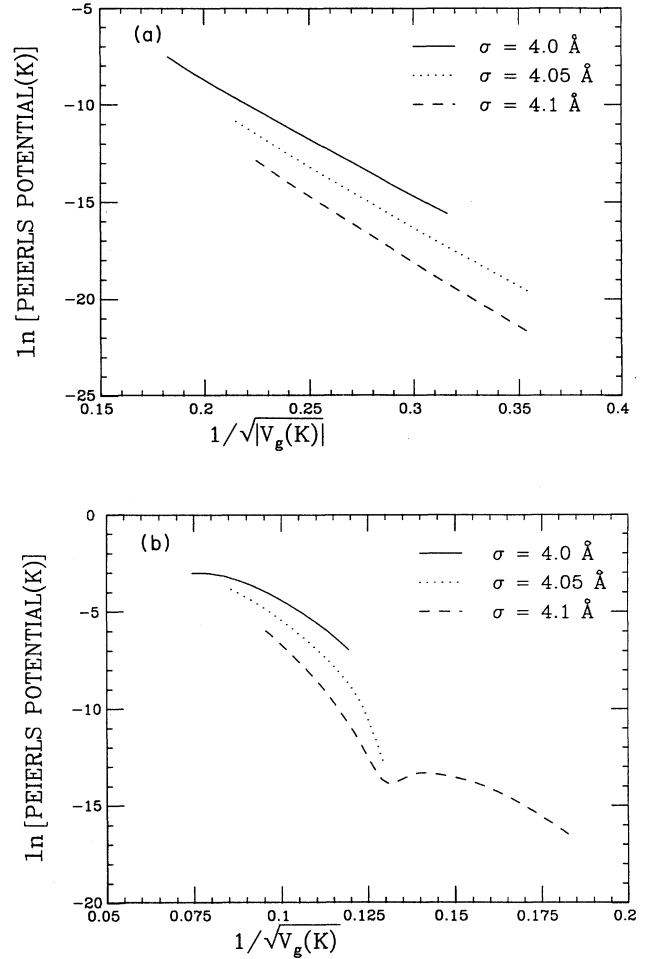


FIG. 10. Dependence of the Peierls barrier potential energy V_{Peierls} on the corrugation V_g . Domains of size $l=48$. For the Frenkel-Kontorova chain the asymptotic behavior is $\ln V_{\text{Peierls}} \propto 1/\sqrt{V_g}$. The location of the cusp for $V_g > 0$ cases is correlated with an interchange of the stable-unstable configurations as the minimum-energy structure (Refs. 13 and 21). (a) $V_g < 0$; (b) $V_g > 0$.

TABLE I. Corrugation amplitude to reproduce C-UIC transitions.^a

σ^b	$V_g > 0$			$V_g < 0$				
	$\sqrt{3}^c$	$\Delta\mu^d$		$\sqrt{3}^c$	$\Delta\mu^d$			
		350	250	150	350	250	150	
4.0	98.2	178	151	122	-8.55	-15.2	-11.5	-7.72
4.05	58.8	120	96.2	71.6	-5.26	-10.0	-7.12	-4.38
4.1	28.1	69.7	49.5	29.6	-2.86	-5.82	-3.76	-1.90

^aAmplitude, in K, of the two-dimensional approximation to the adatom-substrate potential, Eq. (2.3). All entries based on free energies calculated in the quasiharmonic approximation.

^bCharacteristic length, in Å, of the Lennard-Jones (12,6) pair potential, Eq. (2.2). The energy scale is $\epsilon = 230$ K, the atomic mass is for xenon, and the commensurate lattice spacing is 4.80 Å, for Pt(111).

^cAmplitude chosen, by interpolation in the model calculations, to yield a UIC-C transition at $T=50$ K.

^dAmplitude chosen, by interpolation in the model calculations, to yield the C-UIC transition at 70 K after increase of chemical potential (in K) from the value at monolayer condensation by the specified amount; see Sec. III C of the text.

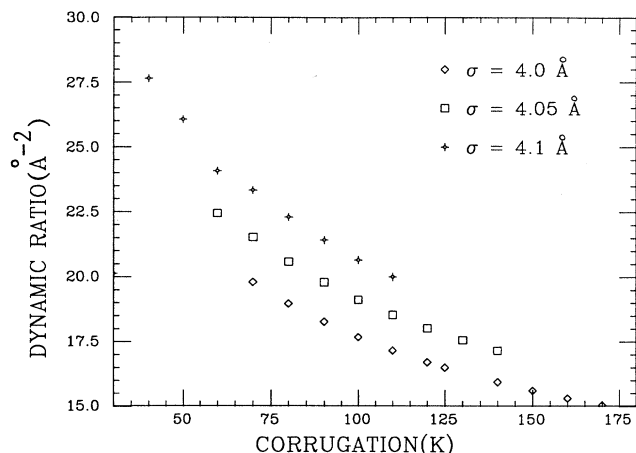


FIG. 11. Dynamic ratio as a function of V_g . The ratio of the square of the minimum zone-center frequency to the Peierls energy, defined in Eq. (3.8), is shown for domains of size $l=48$ for $V_g > 0$. Although the Peierls energy, shown in Fig. 10(b), varies by a factor of 10^4 on this range, the dynamic ratio varies by less than a factor of 2.

energy V_{Peierls} varies over several decades for the corrugation amplitudes used in Fig. 11, but the ratio varies by less than a factor of 2. The zone-center frequency also is informative about the dynamical stability of the UIC lattice: with these constructions for the stable-unstable configurations, the smallest eigenvalue of the dynamical matrix occurs in positive-negative pairs. This was also observed by Black and Mills¹³ in their studies.²¹

Figure 12 shows the frequency spectrum of the UIC lattice for a $V_g < 0$ case, for wave vectors parallel to the direction of the mean misfit. The many branches of the spectrum of the superlattice cell are unfolded to become two branches for wave vectors in the first Brillouin zone of the corresponding UIC lattice. In this case, the polarizations of the two branches are precisely transverse and longitudinal. The frequencies just above the first Brillouin-zone boundary of the superlattice are very close to the frequencies for the commensurate lattice at zero wave vector.²⁴ At intermediate wave vectors there are small gaps in the frequency spectrum again at superlattice zone boundaries. The features which occur for wave vectors near the edge of the uniform UIC lattice Brillouin zone are associated with localized motions of the adatoms in the highly compressed centers of the domain walls, as confirmed by analysis of the eigenvectors of the dynamical matrix.

IV. CONCLUDING REMARKS

This paper presents results of an extensive computational study of the uniaxial incommensurate lattice of a rare-gas monolayer solid. Systematic studies of the Peierls barrier energy and the frequency spectrum of a physisorbed UIC monolayer are given. The development of a gap in the frequency spectrum at the Brillouin zone

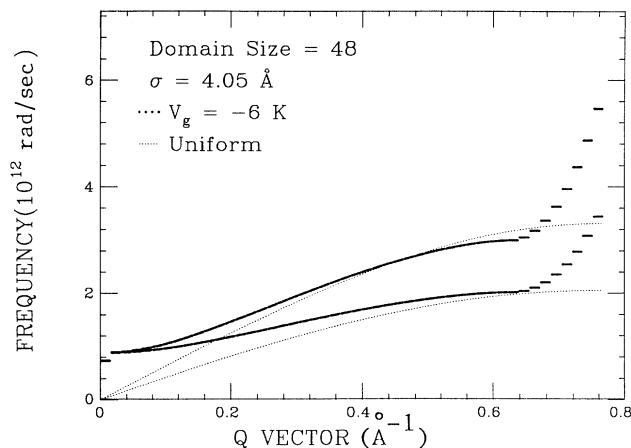


FIG. 12. Frequency spectrum in the extended zone scheme of the superlattice for wave vectors in the direction of mean misfit. UIC lattice of $l=48$, $\sigma=4.05$ Å, and $V_g = -6$ K. The many branches of the superlattice spectrum are unfolded to become two branches for wave vectors in the first Brillouin zone of the corresponding uniform UIC lattice. The upper and lower branches have longitudinal and transverse polarization, except in the first superlattice Brillouin zone, where they interchange. The two branches of the uniform UIC lattice are shown as dotted lines, for comparison purposes.

center of the superlattice was known already from model calculations for one-dimensional chains of atoms.²⁴ The structure in the spectrum at high frequencies, identified with motions within the domain walls, has not been noted previously.

Extensions of this work should include the three-dimensional character of the adsorbed layer, because the smallest atomic spacings in the adlayer, at the center of the domain walls, correspond to quite compressed structures.

There are several other monolayer phases in physisorbed systems, such as the hexagonal incommensurate nonrotated and rotated solids.^{2,3,10} These calculations treat only the C-UIC relative stability. The stability of the modulated UIC lattice relative to hexagonal incommensurate lattices is also of interest.²⁻⁵

For the UIC lattice at small misfit, excitation of domain-wall meanderings at intermediate temperatures leads^{3,12} to effective wall-wall interactions which are larger than the primarily mechanical interactions treated here. The UIC lattice has not been exhausted as a subject for careful study.

ACKNOWLEDGMENTS

This work was supported in part by the National Science Foundation through Grant No. DMR-88-17761 and by the University of Wisconsin-Madison Graduate School with funds provided by the Wisconsin Alumni Research Foundation.

- ¹P. Bak, D. Mukamel, J. Villain, and K. Wentowska, *Phys. Rev. B* **19**, 1610 (1979).
- ²H. Shiba, *J. Phys. Soc. Jpn.* **48**, 211 (1980).
- ³J. Villain and M. B. Gordon, *Surf. Sci.* **125**, 1 (1983).
- ⁴R. J. Gooding, B. Joos, and B. Bergersen, *Phys. Rev. B* **27**, 7669 (1983).
- ⁵M. B. Gordon and F. Lancon, *J. Phys. C* **18**, 3929 (1985).
- ⁶J. M. Gottlieb, *Phys. Rev. B* **42**, 5377 (1990).
- ⁷M. Kardar and A. N. Berker, *Phys. Rev. Lett.* **48**, 1552 (1982).
- ⁸M. B. Gordon and J. Villain, *J. Phys. C* **18**, 3919 (1985).
- ⁹J. E. Black and A. Janzen, *Phys. Rev. B* **38**, 8494 (1988); **39**, 6238 (1989); *Surf. Sci.* **217**, 199 (1989).
- ¹⁰K. Kern, R. David, P. Zeppenfeld, and G. Comsa, *Surf. Sci.* **195**, 353 (1988).
- ¹¹B. Joos, *Solid State Commun.* **42**, 709 (1982).
- ¹²V. L. Pokrovsky and A. L. Talapov, *Theory of Incommensurate Crystals*, Vol. 1 of *Soviet Scientific Reviews Supplement Series Physics* (Harwood Academic, New York, 1984).
- ¹³J. E. Black and D. L. Mills, *Phys. Rev. B* **42**, 5610 (1990).
- ¹⁴J. M. Gottlieb and L. W. Bruch, following paper, *Phys. Rev. B* **44**, 5759 (1991).
- ¹⁵K. Kern, *Phys. Rev. B* **35**, 8265 (1987).
- ¹⁶S. L. Cunningham, *Phys. Rev. B* **10**, 4988 (1974).
- ¹⁷S. E. Roosevelt, Ph.D. thesis, University of Wisconsin–Madison, 1989.
- ¹⁸W. A. Steele, *Surf. Sci.* **36**, 317 (1973).
- ¹⁹J. E. Müller, *Phys. Rev. Lett.* **65**, 3021 (1990).
- ²⁰G. Horton, in *Rare Gas Solids*, edited by M. L. Klein and J. A. Venables (Academic, London, 1977), Vol. I.
- ²¹Isolated examples are encountered, especially at small l , where the identification of the minimum-energy member of the designated stable-unstable pair reverses, but the pairing of smallest eigenvalue of the dynamical matrix remains. Black and Mills (Ref. 13) also observed this.
- ²²L. W. Bruch, *Surf. Sci.* (to be published).
- ²³P. Bak, *Rep. Prog. Phys.* **45**, 587 (1982).
- ²⁴A. D. Novaco, *Phys. Rev. B* **22**, 1645 (1980); C. de Lange and T. Janssen, *J. Phys. C* **14**, 5269 (1981).